

# Shell model results for $^{47-58}\text{Ca}$ isotopes in the $fp$ , $fp_{g_{9/2}}$ and $fp_{g_{9/2}d_{5/2}}$ model spaces

Bharti Bhoy<sup>1\*</sup>, Praveen C. Srivastava<sup>1†</sup> and Kazunari Kaneko<sup>2‡</sup>

<sup>1</sup>*Department of Physics, Indian Institute of Technology Roorkee, Roorkee 247 667, India and*

<sup>2</sup>*Department of Physics, Kyushu Sangyo University, Fukuoka 813-8503, Japan*

(Dated: March 18, 2020)

We have reported shell-model results for  $^{47-58}\text{Ca}$  isotopes in the  $fp$ ,  $fp_{g_{9/2}}$  and  $fp_{g_{9/2}d_{5/2}}$  model spaces using realistic  $NN$  interaction. We have also performed a systematic shell-model study using interactions derived from in-medium similarity-renormalization group (IM-SRG) targeted for a particular nucleus with chiral  $NN$  and  $3N$  forces. The results obtained are in a reasonable agreement with the available experimental data in  $fp$  model space with  $NN$  interaction. It is shown that the  $g_{9/2}$  and  $d_{5/2}$  orbitals play an important role for heavier neutron-rich  $^{54-58}\text{Ca}$  isotopes, while it is marginal for  $^{47-52}\text{Ca}$ . We have also examined spectroscopic factor strengths using  $NN$  and  $NN + 3N$  interactions for recently available experimental data.

PACS numbers: 21.60.Cs, 21.30.Fe, 21.10.Dr, 27.20.+n, 27.30.+t

## I. INTRODUCTION

The study of neutron-rich calcium isotopes is a topic of ongoing interest to understand the shell evolution and the location of drip line [1–3]. The discovery of  $^{60}\text{Ca}$  and implication for the stability of  $^{70}\text{Ca}$  has been recently reported by RIKEN experimental group in the Ref. [4]. In contrast to *ab initio* calculations including three-body forces and continuum effects predict that  $^{59}\text{Ca}$  [5, 6] is unbound and  $^{60}\text{Ca}$  marginally bound and unbound [7]. The mass measurement of  $^{55-57}\text{Ca}$  [8] confirmed the  $N=34$  subshell closure in  $^{54}\text{Ca}$ . In the recent experiment, the robust characteristic of  $N = 34$  subshell closure has been reported in  $^{52}\text{Ar}$  [9].

The neutron-rich Ca isotopes have been previously investigated by the shell model with  $NN$  and  $NN + 3N$  interactions in  $fp$  and  $fp_{g_{9/2}}$  model spaces [10]. Shell-model calculations show that  $fp_{g_{9/2}}$  model space can reproduce reasonable spectra up to  $N \leq 35$  but fails to explain strong collectivity in nuclei around  $N = 40$ . To reproduce the enhanced collectivity,  $d_{5/2}$  orbital should be included in  $fp_{g_{9/2}}$  model space, because collective behavior can be understood in terms of quasi-SU(3) [11]. The importance of the  $d_{5/2}$  orbital is also reported in Ref. [12]. It has been proposed [13] that for neutron-rich  $fp$ -shell nuclei, the neutrons are excited to the  $sdg$  orbitals coupled to the unfilled  $f_{7/2}$  proton orbital is responsible for a new region of deformation. Recently, the shell-model interpretation of the first spectroscopy of  $^{61}\text{Ti}$  using LNPS interaction for  $fp_{g_{9/2}d_{5/2}}$  model space has been reported by Wimmer *et al.* in Ref. [14]. It has been shown that the ground state configuration is dominated by particle-hole excitations to the  $g_{9/2}$  and  $d_{5/2}$  orbitals. Thus, in the neutron-rich  $fp$  shell nuclei, the inclusion of  $g_{9/2}$  and  $d_{5/2}$  orbitals in the model space

becomes crucial as we approach towards  $N = 40$ .

Earlier, it has been shown that the many-body perturbation theory (MBPT) with three-nucleon forces ( $3N$ ) is very important to explain the spectroscopy of neutron-rich Ca isotopes [15]. In addition, the *ab initio* calculations with other modern approaches: in-medium similarity renormalization group (IM-SRG) and coupled-cluster effective interaction (CCEI) with chiral  $NN$  and  $3N$  forces among valence nucleons are found to describe well the location of drip line [16].

The neutron-rich calcium isotopes are particular attraction for investigating the shell formation. The importance of  $3N$  forces are crucial for explaining spectroscopy of Ca chain as reported in Ref. [10].

Motivated with recent experimental data for spectroscopic factor strengths for Ca isotopes, we perform shell-model calculations with  $NN$  and  $NN + 3N$  interactions. The aim of the present manuscript is to investigate recently available experimental data for spectroscopy and nuclear observables for the Ca isotopes using shell-model calculations with  $NN$  interaction for  $fp$ ,  $fp_{g_{9/2}}$ , and  $fp_{g_{9/2}d_{5/2}}$  model spaces. We have also reported shell model results with  $NN + 3N$  interaction for  $fp$  space. The present study will add more information to earlier theoretical work reported in Refs. [10, 15].

This paper is organized as follows. In Sec. II, we present details of theoretical formalism. Comprehensive discussions are reported in Sec. III. Finally, a summary and conclusions are drawn in Sec. IV.

## II. THEORETICAL FRAMEWORK

We can express the present shell-model effective Hamiltonian in terms of single-particle energies and two-body matrix elements numerically,

$$H = \sum_{\alpha} \varepsilon_{\alpha} \hat{N}_{\alpha} + \frac{1}{4} \sum_{\alpha\beta\delta\gamma JT} \langle j_{\alpha} j_{\beta} | V | j_{\gamma} j_{\delta} \rangle_{JT} A_{JT; j_{\alpha} j_{\beta}}^{\dagger} A_{JT; j_{\delta} j_{\gamma}}, \quad (1)$$

\*E-mail address: charubharti14@gmail.com

†Corresponding author: praveen.srivastava@ph.iit.ac.in

‡E-mail address: kkaneko5319@gmail.com

where  $\alpha = \{nljt\}$  denote the single-particle orbitals and  $\varepsilon_\alpha$  stand for the corresponding single-particle energies.  $\hat{N}_\alpha = \sum_{j_z, t_z} a_{\alpha, j_z, t_z}^\dagger a_{\alpha, j_z, t_z}$  is the particle number operator.  $\langle j_\alpha j_\beta | V | j_\gamma j_\delta \rangle_{JT}$  are the two-body matrix elements coupled to spin  $J$  and isospin  $T$ .  $A_{JT}$  ( $A_{JT}^\dagger$ ) is the fermion pair annihilation (creation) operator.

In the present work, we perform shell-model calculations in  $fp$ ,  $fp g_{9/2}$ , and  $fp g_{9/2} d_{5/2}$  model spaces without any truncation. To diagonalize the matrices, the shell model code KSHELL [17] has been used. The maximum dimension we have diagonalized in the case of  $^{58}\text{Ca}$  for the ground state is  $2.7 \times 10^8$ .

We have taken GXPF1Br+ $V_{MU}$  interaction [18] for all the three model spaces. Since the GXPF1Br+ $V_{MU}$  interaction is made for  $fp g_{9/2} d_{5/2}$  model space, thus while doing calculation for  $fp$  and  $fp g_{9/2}$  model spaces, we allow valence neutrons to occupy in the  $f_{7/2}$ ,  $p_{3/2}$ ,  $f_{5/2}$ ,  $p_{1/2}$  orbitals, and further including  $g_{9/2}$  orbital, respectively. To see the impact of modified single-particle energies on the higher mass side of Ca isotopes, we have also reported shell model results for  $fp g_{9/2}$  model space with modified single-particle energy of  $g_{9/2}$  orbital by increasing it with 2 MeV, corresponding results are shown in figures at the last column. This part of the calculation is denoted by  $(fp g_{9/2})_n$ . The  $fp$ -shell matrix elements are taken from GXPF1Br [19]. The GXPF1Br [19] interaction is modified version of GXPF1B [20] with correction in monopole interaction for  $\langle 0f_{5/2} 1p_{3/2} | V | 0f_{5/2} 1p_{3/2} \rangle_{T=1}$ . The GXPF1B interaction [20] is upgraded version with the modification of five  $T = 1$  two-body matrix elements and the bare single-particle energy which involve the  $1p_{1/2}$  orbital from GXPF1A [21]. The cross-shell two-body interaction between  $fp$  and  $gds$ -shell orbitals are taken from  $V_{MU}$  [22]. In the Hamiltonian (Eq. 1) we have added  $\beta_{c.m.} H_{c.m.}$  term as proposed by Gloeckner and Lawson [23] to remove the spurious center-of-mass motion due to the excitation beyond one major shell in the case of  $fp g_{9/2}$  and  $fp g_{9/2} d_{5/2}$  calculations. We have taken  $\beta_{c.m.} = 10$ . There is no further effect on results of energy levels and occupancy of orbitals by increasing value of  $\beta_{c.m.}$ . Further, all the two-body matrix elements are scaled by  $(A/42)^{-0.3}$  as the mass dependence. We have used the harmonic-oscillator parameter  $\hbar\Omega = 41A^{-1/3}$  for all the calculations. Earlier we have reported the importance of  $g_{9/2}$  orbital in the model space for Mn isotopes in the Ref. [24].

Stroberg *et al.* [16] presented a nucleus-dependent valence-space approach using the IM-SRG, which is normal ordered with respect to a finite-density reference state  $|\Phi\rangle$ . This approach adopts a decoupled valence space Hamiltonian in which occupied orbitals are fractionalized. The effective Hamiltonian can be expressed in terms of single-particle energies and two and three-

body matrix elements, as:

$$H = E_0 + \sum_{ij} f_{ij} \{a_i^\dagger a_j\} + \frac{1}{4} \sum_{ijkl} \Gamma_{ijkl} \{a_i^\dagger a_j^\dagger a_l a_k\} + \frac{1}{36} \sum_{ijklmn} W_{ijklmn} \{a_i^\dagger a_j^\dagger a_k^\dagger a_n a_m a_l\}, \quad (2)$$

where  $E_0$ ,  $f_{ij}$ ,  $\Gamma_{ijkl}$  and  $W_{ijklmn}$  are the normal ordered zero-, one-, two-, and three-body terms, respectively. The normal ordered strings of creation and annihilation operators obey  $\langle \Phi | \{a_i^\dagger \dots a_j\} | \Phi \rangle = 0$ . Here chiral  $NN$  interaction is taken from  $N^3\text{LO}$  [25, 26], and a chiral  $3N$  interaction is taken from  $N^2\text{LO}$  [27]. To make the calculation easier, the residual  $3N$  interaction  $W_{ijklmn}$  is neglected among valence nucleons leading to the normal-ordered two-body approximation.

### III. RESULTS AND DISCUSSION

The comparisons of energy levels with shell model calculations and experimental data are shown for  $^{47-52}\text{Ca}$  and  $^{53-58}\text{Ca}$  in Figs. 1 and 2, respectively.

In  $^{47}\text{Ca}$ , the  $fp$ ,  $fp g_{9/2}$ , and  $fp g_{9/2} d_{5/2}$  model spaces result for negative parity states are in a reasonable agreement with the experimental data.

In  $^{48}\text{Ca}$ , the first excited  $2^+$  state is higher than those of the neighboring Ca nuclei. All the three set of model space results are in a good agreement with the experimental data for positive parity energy states, while the  $3^-$  and  $5^-$  states in  $fp g_{9/2}$  and  $fp g_{9/2} d_{5/2}$  calculation are much higher than the experimental data. With increasing model space the energy levels are slightly compressing.

For  $^{49}\text{Ca}$ , all the calculations with  $NN$  force reproduce well first excited  $1/2^-$  state. The ground state in  $^{49}\text{Ca}$  is dominated by the single-particle  $p_{3/2}$  state. The calculated first  $5/2^+$  level is at 6.966 MeV in the calculations from  $fp g_{9/2} d_{5/2}$  model space and 9.575 MeV with  $fp g_{9/2}$  model space. For the other excited states, the calculation from all the three valence spaces reproduce reasonably energy levels. In IM-SRG, the first excited  $1/2^-$  state lies at very high energy ( $\sim 1.7$  MeV higher).

For  $^{50}\text{Ca}$ , the location of the first excited state  $2^+$  in all the calculations have been predicted very well with experimental data except for IM-SRG result. IM-SRG calculations with  $NN+3N$  forces underestimate the first excited state by 500 keV. Most of the experimental levels are tentative in case of  $^{50}\text{Ca}$ . The large energy difference between the  $2_1^+$  and  $2_2^+$  states is reproduced by all  $NN$  interactions. The spin and parity of the third excited state have not been experimentally identified, but our calculations predict it  $1^+$  state.

In  $^{51}\text{Ca}$ , there is no definite experimental information on the spins and parities of the excited states. The first excited  $1/2^-$  state is indicative of the effective  $p_{3/2} - p_{1/2}$

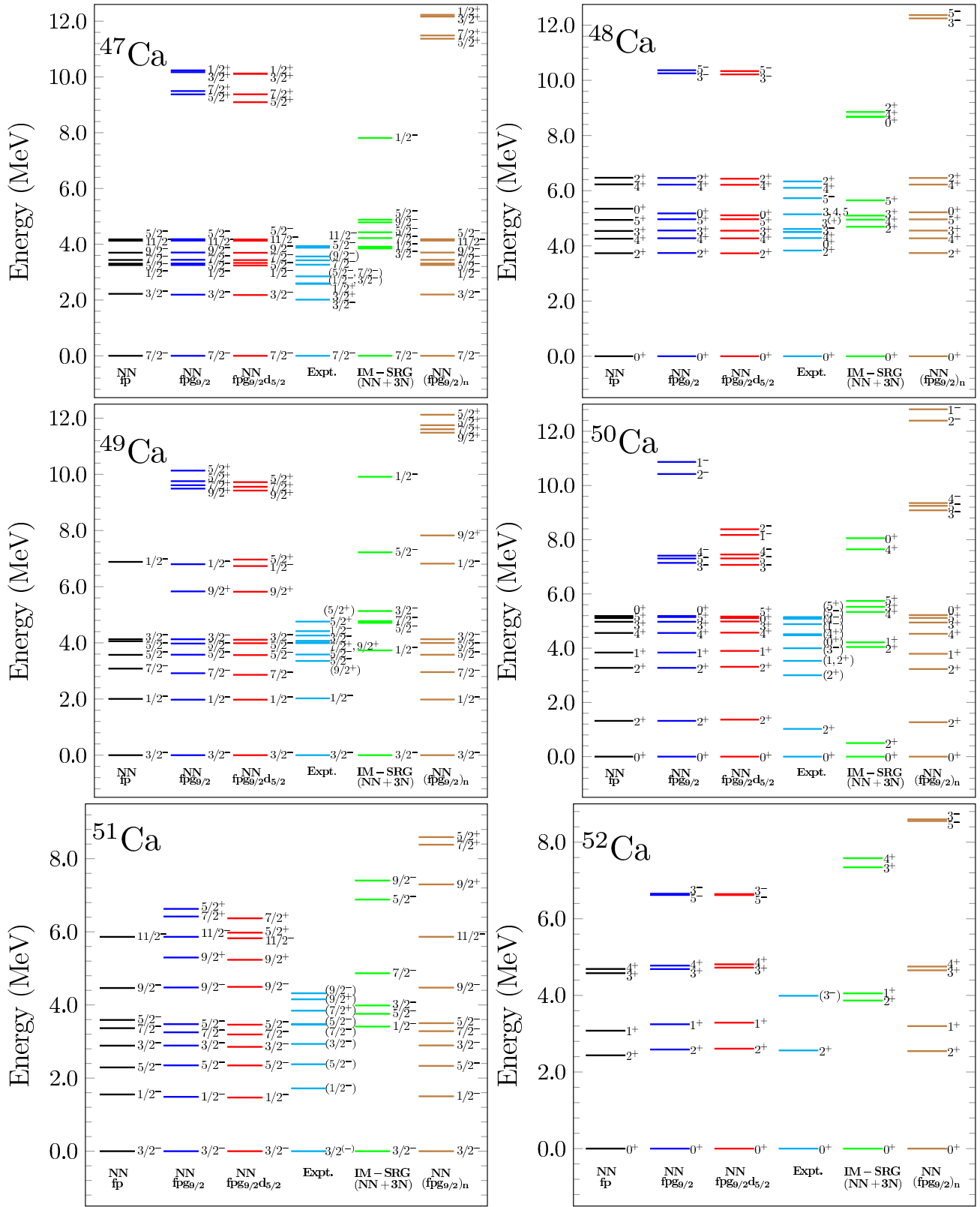


FIG. 1: Comparison between calculated and experimental [29] energy levels for  $^{47-52}\text{Ca}$ .

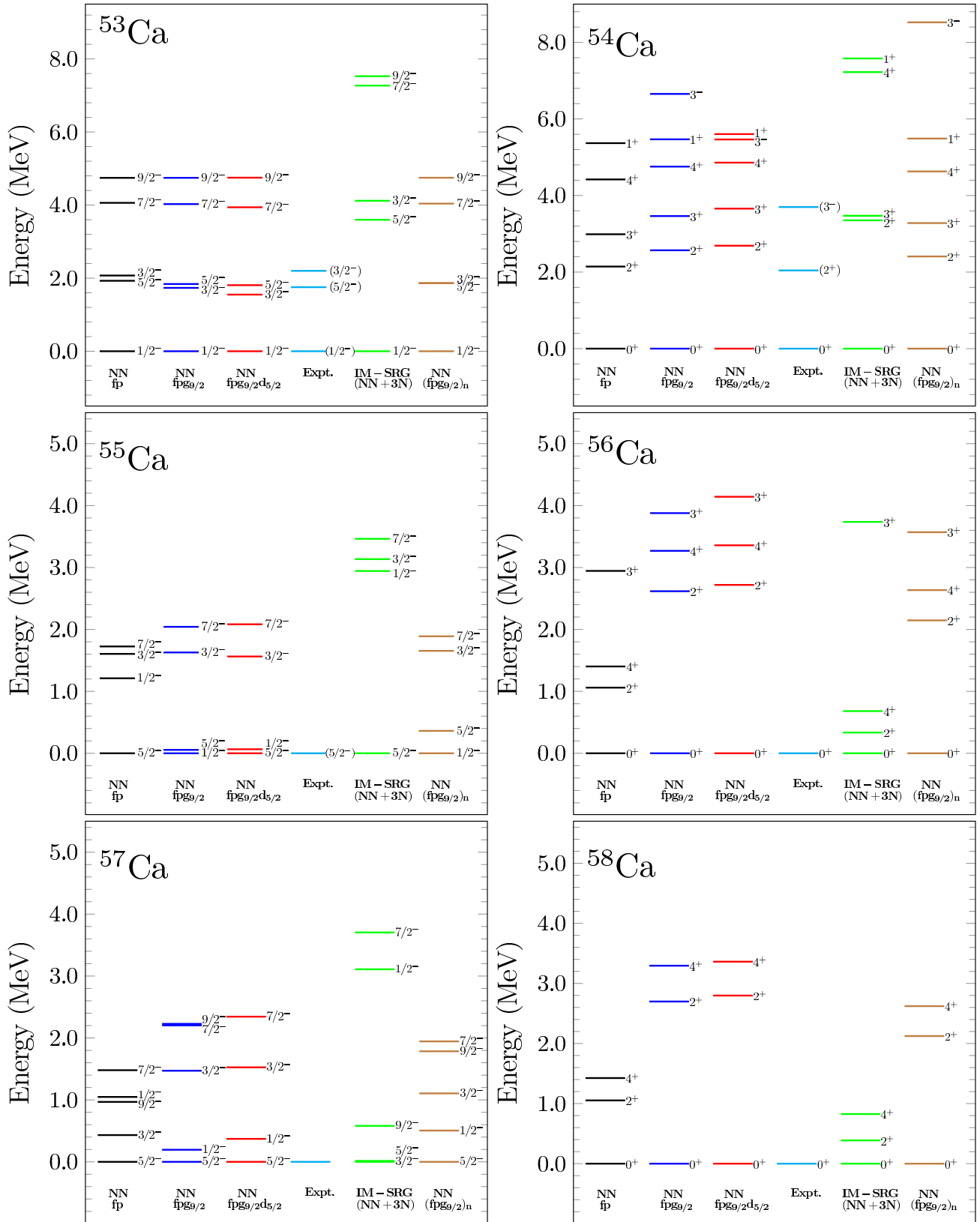


FIG. 2: Comparison between calculated and experimental [29] energy levels for  $^{53-58}\text{Ca}$ .

gap and is consistent with the experimental tentative spin assignment.

The experimental evidence of  $N = 32$  subshell closure for  $^{52}\text{Ca}$  was first time reported in Ref [28]. The calculation from all three valence space reproduces well higher  $2_1^+$  level, consistent with the  $N = 32$  subshell closure. All the calculations predict the second excited state as  $1^+$ , while this state is not yet observed experimentally. The observed ( $3^-$ ) state above  $2_1^+$  is tentative.

In  $^{53}\text{Ca}$ , the ground state is dominated by  $p_{1/2}$  hole. Hence the difference between the first excited  $5/2^-$  and  $3/2^-$  levels will be mostly due to effective  $p_{1/2} - f_{5/2}$  and  $p_{1/2} - p_{3/2}$  gaps. This suggests both the  $N = 32$  and  $N = 34$  subshell closures. The  $fp$ ,  $(fpg_{9/2})_n$  model space and IM-SRG calculations in  $fp$  shell predict  $5/2^-$  for the first excited state. In the valence spaces  $fpg_{9/2}$  and  $fpg_{9/2}d_{5/2}$ , the calculations predict  $3/2^-$ . The calculation from  $(fpg_{9/2})_n$  predicting  $5/2^-$  (1.863 MeV) and  $3/2^-$  (1.865 MeV) levels as almost degenerate.

For  $^{54}\text{Ca}$ , the first experimental spectroscopic study on low-lying states was performed with proton-knockout reactions at RIKEN [19]. They observed  $2_1^+$  state at 2.043 MeV. The calculations predict this state at 2.689 MeV in  $fpg_{9/2}d_{5/2}$  space and at 2.569 MeV in  $fpg_{9/2}$  space and at 2.408 MeV in  $(fpg_{9/2})_n$  space. In the IM-SRG calculation, the first excited state lies much higher (at 3.352 MeV) than the experimental energy.

In  $^{55-58}\text{Ca}$ , only spin and parity of ground states are known except for  $^{57}\text{Ca}$ . We have calculated a few low-lying states using the shell-model. Our calculated results will be important for upcoming future experiments.

In  $^{55}\text{Ca}$   $fp$ ,  $fpg_{9/2}d_{5/2}$ , and IM-SRG predict  $5/2^-$  as ground state, consistent with experimental data.

For  $^{56,58}\text{Ca}$  the first excited  $2^+$  states are at high energy. As  $^{54}\text{Ca}$  is a doubly closed shell nucleus, a  $5/2^-$  state is expected as a ground state for  $^{55}\text{Ca}$ , with excited states at higher energies. This agrees with the results from the  $fp$ ,  $fpg_{9/2}d_{5/2}$  and IM-SRG, but contrasts with the  $fpg_{9/2}$  model space results. The  $fpg_{9/2}d_{5/2}$  calculation predicts a very high  $2^+$  state in  $^{56}\text{Ca}$  at about 2.5 MeV, higher energy than doubly magic isotopes  $^{52}\text{Ca}$  and  $^{54}\text{Ca}$ . In  $^{58}\text{Ca}$ , with a  $2^+$  state around 3 MeV excitation energy. To overcome this problem we have tried to modify the single-particle energy of  $g_{9/2}$  orbital from 0.881 MeV to 2.881 MeV. We chose this particular energy from a series of different sets of calculation with modifying single-particle energy taking reference of  $2^+$  state in  $^{52}\text{Ca}$ . The calculation from  $(fpg_{9/2})_n$  shows that the  $g_{9/2}$  orbital is crucial for higher mass region of Ca isotopes. With the modification of the single-particle energy value of  $g_{9/2}$  orbital, the high  $2^+$  state starts decreasing from  $^{54}\text{Ca}$  onwards, however, it show negligible effect below  $^{54}\text{Ca}$ . The energy levels with IM-SRG is stretched because  $NN$  and  $3N$  forces for this interaction were not consistently SRG evolved.

Thus we may conclude that results of  $fp$  model space is sufficient to reproduce energy levels of  $^{47-52}\text{Ca}$  isotopes

TABLE I:  $B(E2)$  value in calcium isotopes compared with experiment [30, 31]. The  $B(E2)$  values are calculated with IM-SRG and GXPF1Br+VMU ( $fp$ ,  $fpg_{9/2}$ , and  $fpg_{9/2}d_{5/2}$  model spaces) interactions. The units are in  $e^2\text{fm}^4$ .

Nuclei	Transition	Expt.	$fp$	$fpg_{9/2}$	$fpg_{9/2}d_{5/2}$	IM-SRG
$^{47}\text{Ca}$	$3/2^- \rightarrow 7/2^-$	$4.0 \pm 0.2$	3.22	3.08	3.02	1.58
$^{48}\text{Ca}$	$2^+ \rightarrow 0^+$	$19 \pm 6.4$	10.35	10.50	10.60	11.82
$^{49}\text{Ca}$	$7/2^- \rightarrow 3/2^-$	$0.53 \pm 0.21$	3.53	3.27	3.28	0.001
$^{50}\text{Ca}$	$2^+ \rightarrow 0^+$	$7.4 \pm 0.2$	7.82	7.82	8.01	8.0
$^{51}\text{Ca}$	$7/2^- \rightarrow 3/2^-$	N/A	6.72	6.44	6.43	7.64
$^{52}\text{Ca}$	$2^+ \rightarrow 0^+$	N/A	6.16	6.67	7.06	6.46
$^{53}\text{Ca}$	$7/2^- \rightarrow 3/2^-$	N/A	4.48	5.28	6.10	2.09
$^{54}\text{Ca}$	$2^+ \rightarrow 0^+$	N/A	6.34	7.95	8.55	6.13
$^{55}\text{Ca}$	$7/2^- \rightarrow 3/2^-$	N/A	5.39	2.69	2.02	4.55
$^{56}\text{Ca}$	$2^+ \rightarrow 0^+$	N/A	8.95	13.15	13.92	6.90
$^{58}\text{Ca}$	$2^+ \rightarrow 0^+$	N/A	8.25	10.48	11.12	6.85

and the role of  $d_{5/2}$  orbital is very small. Although, with increasing the neutron number, occupancies of the  $g_{9/2}$  and  $d_{5/2}$  orbitals increase as shown in the Fig. 3. The occupancies for  $g_{9/2}$  and  $d_{5/2}$  decrease for the excited states. This means the effects of  $g_{9/2}$  and  $d_{5/2}$  could become important for  $B(E2)$  between the ground state and the first excited state beyond  $^{54}\text{Ca}$ . In fact, as seen in Table I, the  $B(E2)$  increases for  $fpg_{9/2}$  and  $fpg_{9/2}d_{5/2}$  model space beyond  $^{52}\text{Ca}$ , while they are almost similar to all model spaces below  $^{52}\text{Ca}$ .

In Table I, we have shown  $B(E2)$  values for transitions in Ca isotopes. Our calculated results are in a reasonable agreement with the available experimental data. In the calculations, the neutron effective charge is taken as  $e_n = 0.5e$ . It is clearly seen in Table I that the  $g_{9/2}$  and  $d_{5/2}$  orbitals affect significantly the  $B(E2)$  values for heavier  $^{54-58}\text{Ca}$ . Thus the  $g_{9/2}$  and  $d_{5/2}$  orbitals play an important role for  $^{54-58}\text{Ca}$ .

In Table II, we present the calculated spectroscopic quadrupole moments and magnetic moments for odd-mass of calcium isotopes using GXPF1Br+VMU ( $fp$ ,  $fpg_{9/2}$ ,  $fpg_{9/2}d_{5/2}$  model spaces) and IM-SRG ( $fp$ ) interactions. The overall calculated results are in good agreement with the experimental data for magnetic moments. For  $^{53,55,57}\text{Ca}$ , the experimental data are not available. For  $^{47,49,51}\text{Ca}$  isotopes, the single particle magnetic moment value is -1.913 corresponding to the last filled neutron in  $f_{7/2}$  ( $^{47}\text{Ca}$ ) and  $p_{3/2}$  ( $^{49,51}\text{Ca}$ ) orbitals. The calculated magnetic moments of  $^{47}\text{Ca}$  and  $^{49}\text{Ca}$  are somewhat close to the effective single particle moment, indicating less contribution of the higher orbitals. For  $^{51}\text{Ca}$  the difference in the single particle magnetic moment and theoretical calculation is large, showing collective effect of orbitals. For the  $^{53,55,57}\text{Ca}$  isotopes, the single particle magnetic moment corresponding to the last occupied orbital  $f_{5/2}$  is +1.366. For  $^{53}\text{Ca}$ , the magnetic moment value is very less than the single particle magnetic moment, this shows that the ground state for this isotope has a mixed configuration. In the case of  $^{55}\text{Ca}$

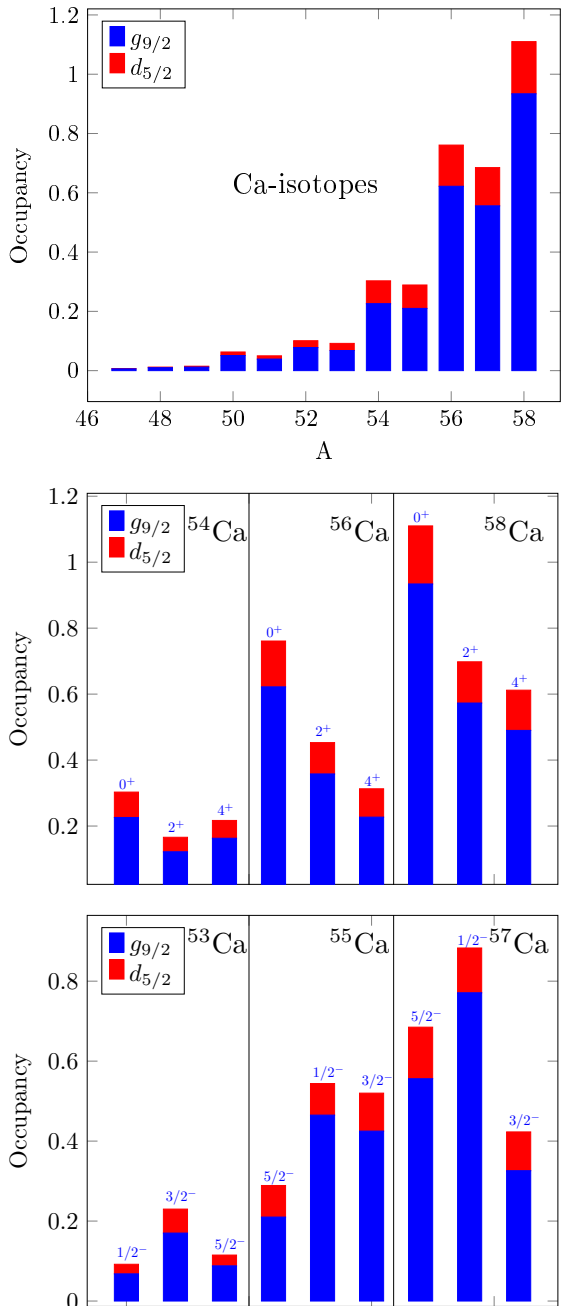


FIG. 3: Occupancies of  $g_{9/2}$  and  $d_{5/2}$  orbitals for the ground and excited states in the Ca isotopes with GXPF1Br+ $V_{MU}$  interaction. In the first graph the occupancy of only ground states are shown.

for  $fp_{g_{9/2}}$  interaction there is a drop in magnetic moment value, which maybe related to the ground state prediction, here we have shown value for the  $5/2^-$  state, for the obtained ground state  $1/2^-$  (from SM) also magnetic moment value is very small 0.2249. The magnetic

moment values obtained from all the interactions are almost same for  $^{47,49,51}\text{Ca}$  isotopes. For  $^{57}\text{Ca}$  calculated magnetic moment value becomes close to single particle magnetic moment for the  $fp_{g_{9/2}d_{5/2}}$  interaction. In the case of  $^{57}\text{Ca}$  the calculated magnetic moment for  $5/2^-$  state is larger with  $fp_{g_{9/2}d_{5/2}}$  model space in comparison to  $fp$  and  $fp_{g_{9/2}}$  model spaces. This reflects the effect of inclusion of  $d_{5/2}$  orbital in the model space.

The calculated spectroscopic quadrupole moments are also compared to the known experimental values. Here we can see, a good description of the data has been obtained from all the interactions. The value of single particle quadrupole moment (in  $eb$ ) for  $^{47,49,51,53,55,57}\text{Ca}$  isotopes are 0.075, -0.046, 0.047, -0.049, -0.071, 0.073, respectively. Since single particle quadrupole moments are not very close to the experimental quadrupole moment for  $^{47,49,51}\text{Ca}$ , thus we may conclude that the single particle contribution is not very strong for these isotopes, although there is a small configuration mixing. The IM-SRG interaction values are much closer to the single particle quadrupole moment. For  $^{55}\text{Ca}$  and  $^{57}\text{Ca}$  isotopes calculated quadrupole moments are very less than the single particle quadrupole moments.

Next, we study spectroscopic factor strengths  $C^2S$  associated with neutron-hole states in  $^{47-53}\text{Ca}$  from IM-SRG and GXPF1Br+ $V_{MU}$  ( $fp$ ,  $fp_{g_{9/2}}$ , and  $fp_{g_{9/2}d_{5/2}}$  model spaces) interactions. Experimental data are available for  $^{48}\text{Ca} \rightarrow ^{47}\text{Ca}$  and  $^{50}\text{Ca} \rightarrow ^{49}\text{Ca}$  transitions. The calculated results are compared with the experimental data [32] in Table III. For the  $^{48}\text{Ca} \rightarrow ^{47}\text{Ca}$  transition, IM-SRG result is  $C^2S_{th} = 7.55$  corresponding to observed  $C^2S_{exp} = 6.4^{+0.4}_{-0.9}$  for the lowest  $7/2^-$  state, while GXPF1Br+ $V_{MU}$  is giving  $C^2S_{th} \sim 7.7$ . The calculated spectroscopic factor to the first excited  $3/2^-$  state is too small in comparison with the experimental value. For  $^{50}\text{Ca} \rightarrow ^{49}\text{Ca}$ , the spectroscopic factor from the IM-SRG for the  $3/2^-$  and  $7/2^-$  states are reasonable as in the experimental data, while it is quite small for the  $1/2^-$  state. From GXPF1Br+ $V_{MU}$  interaction the spectroscopic factor for the  $3/2^-$  and  $1/2^-$  states are reasonable as in the experimental data and giving a large value for  $7/2^-$  state. For  $^{52}\text{Ca} \rightarrow ^{51}\text{Ca}$  and  $^{54}\text{Ca} \rightarrow ^{53}\text{Ca}$  transitions, we have reported theoretical results of the spectroscopic factor for future experiment. Recently, the ab initio calculation for  $C^2S$  corresponding to  $^{54}\text{Ca} \rightarrow ^{53}\text{Ca}$  transition using  $N2LO_{sat}$  and  $NN + 3N$  (lnl) interactions are reported in the Ref. [34]. In the present work, we have compared our calculated results with these ab initio results in the Table I. The ab initio  $C^2S$  [34] are lower than the GXPF1 ones because due to collective excitations. Our results for  $C^2S$  also become smaller once we increase model space from  $fp$  to  $fp_{g_{9/2}}$  to  $fp_{g_{9/2}d_{5/2}}$ .

The poor spectroscopy produced by the IM-SRG might be due to (i) if we look Stroberg et al. [16], in the Fig. 2, the calcium isotopes around  $^{48}\text{Ca}$  are overbound by something like 50 MeV. This is due to at least in part to the fact that the  $NN$  and  $3N$  forces for this interaction were not consistently SRG evolved. The inconsistent evo-

TABLE II: Comparison of experimental [33] and theoretical quadrupole and magnetic moments of ground states. Shell model results obtained from IM-SRG and GXPF1Br+ $V_{MU}$  ( $fp$ ,  $fp_{g9/2}$ , and  $fp_{g9/2}d_{5/2}$  model spaces) interactions. We have taken  $e_n = 0.5e$  and  $g_s^{eff} = g_s^{free}$ .

A	$J^\pi$	$\mu(\mu_N)$				Q(eb)					
		Expt.	$fp$	$fp_{g9/2}$	$fp_{g9/2}d_{5/2}$	IM-SRG	Expt.	$fp$	$fp_{g9/2}$	$fp_{g9/2}d_{5/2}$	IM-SRG
47	$7/2^-$	-1.4064(11)	-1.4618	-1.4661	-1.4679	-1.3640	+0.084(6)	+0.0675	+0.0673	+0.0675	+0.0790
49	$3/2^-$	-1.3799(8)	-1.3921	-1.3919	-1.3857	-1.3290	-0.0360(3)	-0.0386	-0.0386	-0.0386	-0.0452
51	$3/2^-$	-1.0496(11)	-1.0077	-1.0503	-1.0523	-1.0610	+0.036(12)	+0.0390	+0.0371	+0.0369	+0.0421
53	$1/2^-$	N/A	+0.5063	+0.5120	+0.5020	+0.4930					
55	$5/2^-$	N/A	+1.0687	+0.3617 <sup>a</sup>	+1.0316	+0.9870	N/A	-0.0550	-0.0476 <sup>b</sup>	-0.0482	-0.0567
57	$5/2^-$	N/A	+0.486	+0.472	+1.1668	+1.176 <sup>c</sup>	N/A	+0.003	+0.001	+0.001	-0.0012 <sup>d</sup>

<sup>a</sup>Although  $1/2^-$  predicted as a g.s. from SM

<sup>b</sup>Although  $1/2^-$  predicted as a g.s. from SM

<sup>c</sup>Although  $3/2^-$  predicted as a g.s. from SM

<sup>d</sup>Although  $3/2^-$  predicted as a g.s. from SM

TABLE III: Comparison of experimental [32] and theoretical spectroscopic factor strengths obtained from IM-SRG and GXPF1Br+ $V_{MU}$  ( $fp$ ,  $fp_{g9/2}$ , and  $fp_{g9/2}d_{5/2}$  model spaces) interactions for different transitions.

Level energy (keV)	$J^\pi$	$C^2S_{exp}$	IM-SRG	$fp$	$fp_{g9/2}$	$fp_{g9/2}d_{5/2}$	N2LO <sub>sat</sub> [34]	NN + 3N (lnl) [34]
<sup>48</sup> Ca → <sup>47</sup> Ca								
0	$7/2^-$	$6.4_{-0.9}^{+0.8}$	7.5	7.7	7.6	7.6		
2014	$3/2^-$	$\leq 1.4$	0.002	0.05	0.05	0.06		
<sup>50</sup> Ca → <sup>49</sup> Ca								
0	$3/2^-$	2.1(3)	1.8	1.8	1.7	1.6		
2023	$1/2^-$	$0.28_{-0.03}^{+0.05}$	0.04	0.09	0.1	0.1		
3357[32]	$7/2^-$	$3.4_{-0.3}^{+0.4}$	4.7	7.7	7.6	7.6		
<sup>52</sup> Ca → <sup>51</sup> Ca								
0	$3/2^-$	N/A	3.7	3.5	3.4	3.3		
1718	$1/2^-$	N/A	0.04	0.1	0.1	0.2		
2378	$5/2^-$	N/A	0.003	0.003	0.01	0.01		
<sup>54</sup> Ca → <sup>53</sup> Ca								
0	$1/2^-$	N/A	1.9	1.8	1.4	1.3	1.56	1.58
1738[34]	$5/2^-$	N/A	0.01	0.1	0.5	0.5	0.01	0.02
2220[34]	$3/2^-$	N/A	3.8	3.5	3.4	3.4	3.12	3.17

lution led to the oxygen chain agreeing with experiment, but this is almost certainly due to a lucky cancellation for that mass region. As we can see, the C isotopes are underbound and the Ca and Ni are overbound. (ii) also inadequacies of the initial chiral EFT interaction, in the Ref. [35] it is reported that the way that the  $3N$  force was fit for that interaction was a mistake. Basically, it was fit to the beta decay of the triton, but an incorrect conversion between the axial current and the  $3N$  coupling was used.

Previously, shell-model calculation for Ca isotopes has been done in Ref. [10] with many-body perturbation theory (MBPT) using  $NN + 3N$  forces in the extended model space  $pf_{g9/2}$ . In our present work, we have tried to get better energy spectra for neutron-rich calcium isotopes along with nuclear observables. As the result reported in Ref. [10], energy spectra is very much compressed from <sup>47</sup>Ca to <sup>49</sup>Ca, although after

inclusion of  $3N$  forces, somehow it improves but still gives approximately 1~2 MeV compressed spectra. In our calculations up to <sup>54</sup>Ca where experimental data are known, we can obtain very reasonable energy spectra for natural parity states. The calculation from MBPT contrary to experiment giving  $0^+$  as the first excited state in <sup>48</sup>Ca and <sup>54</sup>Ca. In the present work, we have  $2^+$  as the first excited state in <sup>48</sup>Ca and <sup>54</sup>Ca as in the experimental data at similar energy difference from the g.s. In comparison with the Ref. [10], our calculation predicts both  $N=32$  and  $34$  subshell closure very well. Also, the calculated first and second excited states of <sup>51</sup>Ca and <sup>53</sup>Ca suggest the subshell closure at  $N=32$  and  $34$ .

TABLE IV: The calculated shell model wave functions corresponding to  $3^-$  state in  $^{48,50,52,54}\text{Ca}$  isotopes.

Nuclei	State	$fp_{g9/2}$	$(fp_{g9/2})_n$	$fp_{g9/2}d_{5/2}$
$^{48}\text{Ca}$	$3^-$	91% $f_{7/2}^7 g_{9/2}^1$	91% $f_{7/2}^7 g_{9/2}^1$	90% $f_{7/2}^7 g_{9/2}^1$
		3.4% $f_{7/2}^6 p_{3/2}^1 g_{9/2}^1$	3.5% $f_{7/2}^6 p_{3/2}^1 g_{9/2}^1$	3.7% $f_{7/2}^6 p_{3/2}^1 g_{9/2}^1$
		1.5% $f_{7/2}^5 p_{3/2}^2 g_{9/2}^1$	1.5% $f_{7/2}^5 p_{3/2}^2 g_{9/2}^1$	1.5% $f_{7/2}^5 p_{3/2}^2 g_{9/2}^1$
$^{50}\text{Ca}$	$3^-$	93.8% $f_{7/2}^8 p_{3/2}^1 g_{9/2}^1$	93.3% $f_{7/2}^8 p_{3/2}^1 g_{9/2}^1$	87% $f_{7/2}^8 p_{3/2}^1 g_{9/2}^1$
		1.4% $f_{7/2}^6 p_{3/2}^3 g_{9/2}^1$	1.4% $f_{7/2}^6 p_{3/2}^3 g_{9/2}^1$	2.6% $f_{7/2}^8 p_{3/2}^1 d_{5/2}^1$
		1.1% $f_{7/2}^6 p_{3/2}^1 f_{5/2}^2 g_{9/2}^1$	1.1% $f_{7/2}^6 p_{3/2}^1 f_{5/2}^2 g_{9/2}^1$	1.6% $f_{7/2}^6 p_{3/2}^2 g_{9/2}^1$
$^{52}\text{Ca}$	$3^-$	87% $f_{7/2}^8 p_{3/2}^3 g_{9/2}^1$	88% $f_{7/2}^8 p_{3/2}^3 g_{9/2}^1$	83.5% $f_{7/2}^8 p_{3/2}^3 g_{9/2}^1$
		3.3% $f_{7/2}^8 p_{3/2}^1 p_{1/2}^2 g_{9/2}^1$	3.2% $f_{7/2}^8 p_{3/2}^1 p_{1/2}^2 g_{9/2}^1$	3.7% $f_{7/2}^8 p_{3/2}^1 p_{1/2}^2 g_{9/2}^1$
		2.5% $f_{7/2}^8 p_{3/2}^1 f_{5/2}^2 g_{9/2}^1$	2.2% $f_{7/2}^8 p_{3/2}^1 f_{5/2}^2 g_{9/2}^1$	2.6% $f_{7/2}^8 p_{3/2}^1 f_{5/2}^2 g_{9/2}^1$
$^{54}\text{Ca}$	$3^-$	77.3% $f_{7/2}^8 p_{3/2}^3 p_{1/2}^2 g_{9/2}^1$	77.5% $f_{7/2}^8 p_{3/2}^3 p_{1/2}^2 g_{9/2}^1$	86.2% $f_{7/2}^8 p_{3/2}^4 p_{1/2}^1 d_{5/2}^1$
		8.7% $f_{7/2}^8 p_{3/2}^3 f_{5/2}^2 g_{9/2}^1$	9.1% $f_{7/2}^8 p_{3/2}^3 f_{5/2}^2 g_{9/2}^1$	3.2% $f_{7/2}^8 p_{3/2}^2 f_{5/2}^2 p_{1/2}^1 d_{5/2}^1$
		3.5% $f_{7/2}^8 p_{3/2}^3 g_{9/2}^1$	2.9% $f_{7/2}^8 p_{3/2}^3 f_{5/2}^2 p_{1/2}^1 g_{9/2}^1$	1.2% $f_{7/2}^6 p_{3/2}^4 f_{5/2}^2 p_{1/2}^1 d_{5/2}^1$

#### IV. EXCITATION ENERGIES OF $3_1^-$ STATE IN EVEN-EVEN CA ISOTOPES

The wave function corresponding to  $3_1^-$  state in the  $^{48,50,52,54}\text{Ca}$  isotopes with  $fp_{g9/2}$  and  $(fp_{g9/2})_n$  interactions are shown in the Table IV. The calculated  $3_1^-$  state for  $^{48,50,52,54}\text{Ca}$  isotopes with  $(fp_{g9/2})_n$  interaction is higher than that of the  $fp_{g9/2}$  interaction due to increase in the single particle energy of  $g_{9/2}$  orbital by 2 MeV. The occupancy of  $p_{3/2}$  orbital is changing from 0.073 ( $^{48}\text{Ca}$ ) to 1.037 ( $^{50}\text{Ca}$ ) to 2.835 ( $^{52}\text{Ca}$ ) to 2.943 ( $^{54}\text{Ca}$ ) with original  $fp_{g9/2}$  interaction. The  $3_1^-$  state is dominated by  $\nu(p_{3/2}^1 g_{9/2}^1)$  configuration.

Since the  $(fp_{g9/2})_n$  interaction predicts  $3_1^-$  state at 12.244 MeV for  $^{48}\text{Ca}$ , the calculated  $J^\pi = 5/2^+$ ,  $7/2^+$  and  $9/2^+$  states around 12 MeV in  $^{49}\text{Ca}$  are the multiplets coming from coupling of  $(3_1^- \otimes p_{3/2}^1)_J$ . Similarly  $(fp_{g9/2})_n$  interaction predicts  $3_1^-$  state at 9.085 MeV for  $^{50}\text{Ca}$ , the multiplets of  $(3_1^- \otimes p_{3/2}^1)_J$  is responsible for  $J^\pi = 5/2^+$ ,  $7/2^+$  and  $9/2^+$  states in  $^{51}\text{Ca}$ .

#### V. CONCLUSIONS

In the present work, we have performed shell-model calculations with realistic  $NN$  interactions for  $^{47-58}\text{Ca}$  isotopes. To see the importance of  $g_{9/2}$  and  $d_{5/2}$  orbitals, we have performed calculations for  $fp$ ,  $fp_{g9/2}$ , and  $fp_{g9/2}d_{5/2}$  model spaces. In our calculations, after  $^{54}\text{Ca}$ , we are getting a very high  $2^+$  state in the case

of  $^{56,58}\text{Ca}$ . Thus, to reduce the energy of  $2^+$  state and to see the importance of  $g_{9/2}$  orbital, we have increased the single-particle energy of this orbital by 2 MeV. With this modification, however, the calculated  $3^-$  states become higher than those of the  $fp_{g9/2}$  calculations. On the other way, it might be also possible to adjust the cross-shell pairing two-body matrix elements (TBMEs)  $\langle (fp)^2 | V | (g_{9/2}d_{5/2})^2 \rangle (J=0)$  to reduce the binding energy of  $0_1^+$ . The  $3^-$  problem remains open question. Results corresponding to the modified single-particle energy shows that  $g_{9/2}$  orbital is very crucial for heavier Ca isotopes. The significant increase of occupancy for the  $g_{9/2}$  orbital is obtained above  $N=34$  once we move towards heavier  $^{54-58}\text{Ca}$  isotopes. The calculations predict that the  $d_{5/2}$  orbital also plays an important role for heavier  $^{54-58}\text{Ca}$ , while it is marginal for  $^{47-52}\text{Ca}$ . Our calculations support  $N=32$  and  $N=34$  subshell closures in the Ca isotopes for  $^{52}\text{Ca}$  and  $^{54}\text{Ca}$ , and also confirmed by the wavefunctions of  $^{53}\text{Ca}$  for ground state, first and second excited states. The results for the IM-SRG interaction targeted for a particular nucleus with chiral  $NN$  and  $3N$  forces are also reported.

#### ACKNOWLEDGEMENTS

B. Bhoj acknowledges financial support from MHRD, Government of India. PCS acknowledges a research grant from SERB (India), CRG/2019/000556. We have performed theoretical calculations at Prayag 5 node computational facility at IIT-Roorkee. PCS would like to thank T. Togashi and R. Stroberg for useful help.

[1] R.F. Garcia Ruiz et al., Unexpectedly large charge radii of neutron-rich calcium isotopes, *Nat. Phys.* **12**, 594

(2016).



- [2] J. D. Holt, S. R. Stroberg, A. Schwenk, and J. Simonis, Ab initio limits of atomic nuclei, [arXiv:1905.10475](https://arxiv.org/abs/1905.10475).
- [3] N. A. Smirnova, B. Bally, K. Heyde, F. Nowacki, K. Sieja, Shell evolution and nuclear forces, *Phys.Lett. B* **686**, 109 (2010).
- [4] O.B. Tarasov et al., Discovery of  $^{60}\text{Ca}$  and Implications For the Stability of  $^{70}\text{Ca}$ , *Phys. Rev. Lett.* **121**, 022501 (2018).
- [5] G. Hagen, M. Hjorth-Jensen, G.R. Jensen and R. Machleidt, and T. Papenbrock, Evolution of Shell Structure in Neutron-Rich Calcium Isotopes, *Phys. Rev. Lett.* **109**, 032502 (2012).
- [6] C. Forssen, G. Hagen, M. Hjorth-Jensen, W. Nazarewicz, and J. Rotureau, Living on the edge of stability, the limits of the nuclear landscape, *Phys. Scr.* **T152**, 014022 (2013).
- [7] G. Hagen, P. Hagen, H.-W. Hammer, and L. Platter, Efimov Physics Around the Neutron-Rich  $^{60}\text{Ca}$  Isotope, *Phys. Rev. Lett.* **111**, 132501 (2013).
- [8] S. Michimasa et al., Magic Nature of Neutrons in  $^{54}\text{Ca}$ : First Mass Measurements of  $^{55-57}\text{Ca}$ , *Phys. Rev. Lett.* **121**, 022506 (2018).
- [9] H.N. Liu et al., How robust is the  $N = 34$  subshell closure? first spectroscopy of  $^{52}\text{Ar}$ , *Phys. Rev. Lett.* **122**, 072502 (2019).
- [10] J. D. Holt, J. Menendez, J. Simonis, and A. Schwenk, Three-nucleon forces and spectroscopy of neutron-rich calcium isotopes, *Phys. Rev. C* **90**, 024312 (2014).
- [11] S. M. Lenzi et al., Island of inversion around  $^{64}\text{Cr}$ , *Phys. Rev. C* **82**, 054301 (2010).
- [12] K Kaneko, Y. Sun, M. Hasegawa and T. Mizusaki, Shell model study of single-particle and collective structure in neutron-rich Cr isotopes, *Phys. Rev. C* **78**, 064312 (2008).
- [13] E. Caurier, F. Nowacki, and A. Poves, Large-scale shell model calculations for exotic nuclei, *Eur. Phys. J. A* **15**, 145-150 (2002).
- [14] K. Wimmer et al., First spectroscopy of  $^{61}\text{Ti}$  and the transition to the island of inversion at  $N = 40$ , *Phys. Lett. B* **792**, 16 (2019).
- [15] J. D. Holt, T. Otsuka, A. Schwenk and T. Suzuki, Three-body forces and shell structure in calcium isotopes, *J. Phys. G: Nucl. Part. Phys.* **39**, 085111 (2012).
- [16] S. R. Stroberg, A. Calci, H. Hergert, J. D. Holt, S. K. Bogner, R. Roth and A. Schwenk, Nucleus-Dependent Valence-Space Approach to Nuclear Structure, *Phys. Rev. Lett.* **118**, 032502 (2017).
- [17] Noritaka Shimizu, Nuclear shell-model code for massive parallel computation, KSHELL (private communication).
- [18] T. Togashi et al., Large-scale shell-model calculations for unnatural-parity high-spin states in neutron-rich Cr and Fe isotopes, *Phys. Rev. C* **91**, 024320 (2015).
- [19] D. Steppenbeck et al., Evidence for a new nuclear magic number from the level structure of  $^{54}\text{Ca}$ , *Nature* **502**, 207 (2013).
- [20] M. Honma et al., Shell-model description of neutron-rich Ca isotopes, *RIKEN Accel. Prog. Rep.* **41**, 32 (2008).
- [21] M. Honma, T. Otsuka, B. A. Brown, and T. Mizusaki, Shell-model description of neutron-rich pf-shell nuclei with a new effective interaction GXPF1, *Eur. Phys. J. A* **25**, 499 (2005).
- [22] T. Otsuka, T. Suzuki, M. Honma, Y. Utsuno, N. Tsunoda, Novel Features of Nuclear Forces and Shell Evolution in Exotic Nuclei, K. Tsukiyama, and M. Hjorth-Jensen, *Phys. Rev. Lett.* **104**, 012501 (2010).
- [23] D. H. Gloeckner and R. D. Lawson, Spurious center-of-mass motion, *Phys. Lett.* **53B**, 313 (1974).
- [24] P.C.Srivastava and I.Mehrotra, Large-scale shell model calculations for odd-odd  $^{58-62}\text{Mn}$  isotopes, *Eur. Phys. J. A* **45**, 185 (2010).
- [25] R. Machleidt and D.R. Entem, Chiral effective field theory and nuclear forces, *Phys. Rep.* **503**, 1 (2011).
- [26] D.R. Entem and R. Machleidt, Accurate charge-dependent nucleon-nucleon potential at fourth order of chiral perturbation theory, *Phys. Rev. C* **68**, 041001(R) (2003).
- [27] P. Navratil, Local three-nucleon interaction from chiral effective field theory, *Few-Body Syst.* **41**, 117 (2007).
- [28] A. Huck, G. Klotz, A. Knipper, C. Miede, C. Richard-Serre, G. Walter, A. Poves, H. L. Ravn, and G. Marguier, Beta decay of the new isotopes  $^{52}\text{K}$ ,  $^{52}\text{Ca}$ , and  $^{52}\text{Sc}$ ; a test of the shell model far from stability, *Phys. Rev. C* **31**, 2226 (1985).
- [29] <http://www.nndc.bnl.gov/ensdf/>.
- [30] D. Montanari, S. Leoni, D. Mengoni, J. J. Valiente-Dobon, G. Benzoni, N. Blasi, G. Bocchi, P. F. Bortignon, S. Bottoni, and A. Bracco,  $\gamma$  spectroscopy of calcium nuclei around doubly magic  $^{48}\text{Ca}$  using heavy-ion transfer reactions, *Phys. Rev. C* **85**, 044301 (2012).
- [31] S. Raman, C. W. G. Nestor Jr., and P. Tikkanen, Tables of E2 transition probabilities from the first  $2^+$  states in even-even nuclei, *At. Data Nucl. Data Tables* **78**, 1 (2001).
- [32] H. L. Crawford, A. O. Macchiavelli, P. Fallon, M. Albers, Unexpected distribution of  $\nu 1f_{7/2}$  strength in  $^{49}\text{Ca}$ , *Phys. Rev. C* **95**, 064317 (2017).
- [33] R.F. Garcia Ruiz et al., Ground-state electromagnetic moments of calcium isotopes, *Phys. Rev. C* **91**, 041304(R) (2015).
- [34] S. Chen et al., Quasifree neutron knockout from  $^{54}\text{Ca}$  corroborates arising  $N = 34$  neutron magic number, *Phys. Rev. Lett.* **123**, 142501 (2019).
- [35] D. Gazit, S. Quaglioni, and P. Navratil, Erratum: Three-Nucleon Low-Energy Constants from the Consistency of Interactions and Currents in Chiral Effective Field Theory *Phys. Rev. C* **122**, 029901(E) (2019).